*Journal of Fundamental and Applied Research* **Vol. 5**, Issue 4 (2025) **20250026**

Received: 20 October 2025 / Accepted: 19 December 2025
Published online: 19 December 2025
© 2025 The Author(s)

# Anisotropic electrical conductivity in magnetized neutron-star crusts

Nurmuxammed Aytimbetov[1, *] and Mardon Abdullaev[2, 3, †]

[1]*Namangan State University, Bobur shokh 161, Namangan 160107, Uzbekistan*
[2]*Institute of Fundamental and Applied Research, National Research University TIIAME, Kori Niyoziy 39, Tashkent 100000, Uzbekistan*
[3]*Institute of Nuclear Physics, Ulugbek 1, Tashkent 100214, Uzbekistan*

**Abstract.** We compute the electrical conductivity tensor of neutron–star crust matter over densities $\rho = 10^9 - 4 \times 10^{11}\,\mathrm{g\,cm^{-3}}$ and magnetic fields $B = 10^{12} - 10^{15}\,\mathrm{G}$, using a Boltzmann transport framework with a relaxation–time treatment of electron–ion, phonon, and impurity scattering, including Landau quantization in ultra-strong fields. The longitudinal component $\sigma_\parallel$ remains essentially insensitive to $B$, varying by less than 10% across three orders of magnitude in field strength. In contrast, the transverse component $\sigma_\perp$ decreases by nearly two orders of magnitude as $B$ increases from $10^{13}$ to $10^{15}$ G, reflecting strong magnetic suppression once the magnetization parameter $\omega_B\tau \gtrsim 1$. The Hall component $\sigma_H$ rises steeply with $B$, peaking near $\omega_B\tau \approx 1$ and saturating for higher fields; at $B \gtrsim 10^{14}$ G, it exceeds $\sigma_\perp$ by more than an order of magnitude and approaches $\sigma_\parallel$. These results imply highly anisotropic charge and heat transport in magnetar crusts, with cross-field conduction suppressed by factors of $10^2 - 10^3$ relative to the field-aligned direction. Such anisotropy governs surface temperature distributions, magnetic-field decay, and magneto-thermal evolution in strongly magnetized neutron stars.

**Key words:** Neutron star, conductivity, star crust, magetic field, Landau quantization, Hall conductivity.

## I. INTRODUCTION

Neutron stars are among the most extreme and fascinating objects in the Universe. Formed in the aftermath of supernova explosions, these compact remnants exhibit densities exceeding that of atomic nuclei, magnetic fields trillions of times stronger than Earth's, and surface gravities capable of significantly warping spacetime. Neutron stars, though only $\sim 10km$ in radius, contain solar masses of matter [1]. These unique properties make them exceptional laboratories for studying matter under extreme physical conditions.

The outer layers of a neutron star, particularly the *crust*, play a crucial role in its observable behavior. The crust consists of a solid lattice of neutron-rich nuclei immersed in a degenerate sea of electrons, with free neutrons appearing in deeper layers. The electrical and thermal conductivities of this crustal material govern a wide range of astrophysical phenomena, including the cooling of isolated neutron stars, the decay of magnetic fields, and the excitation of crustal oscillations following magnetar flares or glitches. A precise understanding of transport processes in the crust is therefore essential for interpreting observations and modeling neutron star evolution.

One of the most striking features of neutron stars is their *magnetic fields*. While ordinary pulsars exhibit surface magnetic fields on the order of $10^{12}$ G (gauss)—where $1\,\mathrm{G} = 10^{-4}\,\mathrm{T}$, with T (tesla) being the SI unit of magnetic field—magnetars, an exotic subclass of neutron stars, can possess fields exceeding $10^{15}$ G. In such extreme environments, magnetic fields strongly influence transport properties within the crust. The motion of charged particles, particularly degenerate electrons, is constrained by the Lorentz force, resulting in anisotropic conduction, quantization of energy levels (Landau quantization), and significant deviations from classical transport theory. These effects become especially pronounced when the magnetic field strength exceeds the so-called *critical quantum field*,

$$B_\mathrm{c} = 4.4 \times 10^{13}\,\mathrm{G}, \tag{1}$$

at which the electron cyclotron energy matches its rest mass [2].

* nurmuxammedzaytimbetov@gmail.com
† mardonabdullaev@gmail.com

The study of magnetically influenced conductivity is not purely theoretical. Observations of magnetars reveal unusual X-ray emission properties, variable luminosities, and cooling behaviors that demand advanced modeling of heat and charge transport in the presence of strong magnetic fields. Recent progress in both theoretical modeling and observational astrophysics has thus motivated a renewed focus on the microscopic processes occurring in neutron star crusts.

In this work, we investigate the *effects of intense magnetic fields on the electrical conductivity of neutron star crust matter*. Special emphasis is placed on the anisotropy of conductivity, the influence of magnetic field strength and orientation, and the role of quantizing effects under density and temperature conditions characteristic of different crustal layers. The analysis builds on classical transport theory, with quantum-mechanical corrections incorporated where necessary in the high-field regime.

Unlike previous works such as Potekhin (1996), which primarily examined electron conduction along quantizing magnetic fields up to $B \lesssim 10^{13}\,\mathrm{G}$, the present study extends the relaxation–time formalism into the magnetar regime, considering fields as high as $10^{15}\,\mathrm{G}$. In addition, we compute the full anisotropic conductivity tensor $(\sigma_\parallel, \sigma_\perp, \sigma_H)$ rather than only the longitudinal component, thereby enabling a quantitative assessment of magnetic-field–induced anisotropy in both charge and heat transport. This broader treatment allows us to explore the transition from weakly to strongly magnetized regimes and to quantify how magnetar-level fields reshape crustal conductivity and magneto-thermal evolution.

## II. THEORETICAL BACKGROUND

### A. Structure and Composition of the Neutron Star Crust

A neutron star exhibits a highly stratified internal structure, with the crust playing a decisive role in many observable astrophysical phenomena. The crust extends from the surface, where the density is of the order of $10^6\,\mathrm{g\,cm^{-3}}$, down to the neutron drip threshold, $\rho_{\mathrm{ND}} \simeq 4 \times 10^{11}\,\mathrm{g\,cm^{-3}}$. Beyond this density, neutrons begin to leak out of nuclei, marking the transition to the inner crust.

The crust is conventionally divided into two distinct regions. The *outer crust* is composed of a Coulomb lattice of progressively neutron-rich nuclei embedded in an ultrarelativistic, degenerate electron gas. As depth increases, electron captures drive the nuclei toward more neutron-rich isotopes. The *inner crust* begins at the neutron drip density and consists of nuclei arranged in a lattice, coexisting with degenerate electrons and a gas of free neutrons. At the base of this region, the competition between nuclear and Coulomb forces is expected to generate exotic nuclear configurations, known as "pasta phases" (rods, slabs, bubbles). In both regions, the ultrarelativistic and degenerate electron gas determines the dominant transport properties, particularly thermal and electrical conductivity.

### B. Electrical Conductivity in Dense Matter

The electrical conductivity $\sigma$ of crustal matter is controlled by the scattering of degenerate electrons off lattice ions, phonons, and impurities. In the absence of magnetic fields, the electrical conductivity is isotropic and can be described within the relaxation-time approximation, as given by Eq. (2) [3]:

$$\sigma = \frac{n_e e^2 \tau}{m_e^*}, \tag{2}$$

where $n_e$ is the electron number density, $e$ the elementary charge, $\tau$ the relaxation time (average time between collisions), and $m_e^*$ the effective electron mass.

At low temperatures (compared with the Fermi energy), the principal scattering mechanisms are:

- electron–ion scattering at high densities,
- electron–phonon scattering at elevated temperatures ($T \gtrsim 10^8\,\mathrm{K}$),
- electron–impurity scattering in the presence of compositional inhomogeneities.

The total resistivity follows Matthiessen's rule, with contributions from each scattering process summed linearly.

 Copyright © 2025

### C. Magnetic Field Effects on Conductivity

In the presence of a strong magnetic field, electron motion is confined to helical trajectories around field lines. This introduces pronounced anisotropy into the transport properties, can be described by the conductivity tensor [4]:

$$\sigma = \begin{pmatrix} \sigma_\perp & -\sigma_H & 0 \\ \sigma_H & \sigma_\perp & 0 \\ 0 & 0 & \sigma_\parallel \end{pmatrix}, \tag{3}$$

where $\sigma_\parallel$ is the conductivity along the field, $\sigma_\perp$ the transverse conductivity without Hall deflection, and $\sigma_H$ the Hall conductivity.

The degree of anisotropy is governed by the magnetization parameter defined in Eq. (4)

$$\omega_B \tau = \frac{eB}{m_e^* c} \tau, \tag{4}$$

where $\omega_B$ is the electron cyclotron frequency, $B$ the magnetic field strength, $c$ the speed of light, and $\tau$ the relaxation time. When $\omega_B \tau \ll 1$, magnetic effects are negligible; in the opposite regime, $\omega_B \tau \gg 1$, electrons are strongly magnetized, and cross-field conductivity is significantly suppressed.

### D. Landau Quantization

In ultra-strong magnetic fields, particularly for $B \gtrsim B_c = 4.4 \times 10^{13}\,\mathrm{G}$, the transverse motion of electrons is quantized into Landau levels. The corresponding electron energy spectrum, given by Eq. (5), describes the quantized Landau levels of electrons [4]:

$$E_n = \sqrt{(p_z c)^2 + m_e^2 c^4 \left(1 + 2n \frac{B}{B_c}\right)}, \tag{5}$$

where $n$ denotes the Landau level index and $p_z$ is the momentum parallel to the magnetic field.

In the quantizing regime, when only a few Landau levels are populated, the electron density of states is strongly modified, leading to significant alterations in the conductivity. These quantum effects are particularly relevant for magnetars, where they influence both electrical and thermal transport.

### E. Implications for Neutron Star Observables

The conductivity of crustal matter under strong magnetic fields has direct consequences for observable neutron star behavior:

- **Crustal cooling:** Heat is preferentially conducted along magnetic field lines, leading to anisotropic surface temperature distributions.
- **Magnetic field decay:** The dissipation of crustal currents depends on resistivity, which is inversely proportional to conductivity; anisotropy complicates field evolution.
- **Glitches and oscillations:** Conductivity impacts the buildup and relaxation of stresses within the crust, affecting glitch dynamics and magnetoelastic oscillations [5].

A detailed theoretical description of conductivity in magnetized neutron star crusts is therefore indispensable for interpreting X-ray observations, timing irregularities, and thermal mapping of neutron star surfaces.

## III. METHODS

### A. Overview of the Approach

To explore the impact of magnetic fields on the electrical conductivity of neutron star crusts, we employ a semi-analytical framework grounded in the Boltzmann transport equation under the relaxation-time approximation. The electron system is treated as a relativistic, degenerate Fermi gas embedded within a crystalline lattice of nuclei, consistent with the physical conditions in neutron star crusts.

Copyright © 2025

This approach captures both classical and quantum effects, depending on the field strength and density regime under consideration. The conductivity tensor is evaluated layer by layer, taking into account the dominant scattering mechanisms and, where necessary, the quantization of electron motion in ultra-strong magnetic fields. The external magnetic field is considered as a free parameter, varying in both strength and orientation, thereby encompassing the physical regimes relevant to ordinary pulsars ($B \sim 10^{12}$ G) and magnetars ($B \gtrsim 10^{15}$ G).

### B. Physical Assumptions and Parameters

To retain tractability while preserving physical realism, several simplifying assumptions are adopted. First, the electron gas is treated as fully degenerate, with the equilibrium distribution approximated by a step function for $T \ll E_{\rm F}/k_B$. Second, the high densities typical of the neutron star crust ($\rho \gtrsim 10^9\,{\rm g\,cm^{-3}}$) require the use of relativistic expressions for electron energy and momentum. The ions are assumed to form a static Coulomb lattice, so phonon contributions can be neglected in the low-temperature limit. Each layer of the crust is modeled as a one-component plasma, represented by a single nuclear species (e.g., Fe, Kr, or Se) with fixed charge $Z$ and mass number $A$. Finally, a uniform magnetic field directed along the $z$-axis is applied, with strength varied between $10^{12}$ and $10^{15}$ G to capture the regimes relevant for ordinary pulsars and magnetars.

*Fiducial composition and density.* Unless otherwise stated, we adopt a one–component Coulomb lattice of iron (Fe, $Z = 26$, $A \simeq 56$) with impurity parameter $Q = 0$ as our baseline. A frequently referenced fiducial layer in the outer crust is set at $\rho = 10^{10}\,{\rm g\,cm^{-3}}$, where the electron gas is ultrarelativistic and fully degenerate ($T \ll E_F/k_B$). All conductivity components reported for the "fiducial model" correspond to this (Fe, $\rho = 10^{10}\,{\rm g\,cm^{-3}}$) setup, unless noted [6].

### C. Conductivity Tensor in the Relaxation-Time Approximation

In the presence of a magnetic field, the conductivity becomes anisotropic and is expressed by the tensor form of the Boltzmann transport equation [7]:

$$\sigma_{ij} = \frac{e}{(2\pi)^3} \int v_i v_j \left(-\frac{\partial f_0}{\partial \epsilon}\right) \tau(\epsilon)\, d^3p, \tag{6}$$

where $f_0$ is the equilibrium distribution, $v_i$ are the velocity components, $\tau(\epsilon)$ is the relaxation time, and $\epsilon$ is the electron energy.

For a strongly magnetized, degenerate gas, the tensor simplifies to [8]:

$$\sigma = \begin{pmatrix} \dfrac{\sigma_0}{1+(\omega_B\tau)^2} & -\dfrac{\sigma_0\,\omega_B\tau}{1+(\omega_B\tau)^2} & 0 \\ \dfrac{\sigma_0\,\omega_B\tau}{1+(\omega_B\tau)^2} & \dfrac{\sigma_0}{1+(\omega_B\tau)^2} & 0 \\ 0 & 0 & \sigma_0 \end{pmatrix}, \tag{7}$$

with

$$\sigma_0 = \frac{n_e e^2 \tau}{m_e^*}, \quad \omega_B = \frac{eB}{m_e^* c}.$$

This formalism naturally separates into three components:

$$\sigma_\parallel = \sigma_0, \quad \sigma_\perp = \frac{\sigma_0}{1+(\omega_B\tau)^2}, \quad \sigma_H = \frac{\sigma_0\,\omega_B\tau}{1+(\omega_B\tau)^2}. \tag{8}$$

with $\sigma_0 = n_e e^2\tau/m_e^*$ the field-free conductivity. Thus, $\sigma_\parallel$ remains unaffected by the magnetic field, while $\sigma_\perp$ and $\sigma_H$ depend sensitively on the magnetization parameter $\omega_B\tau$, which governs the crossover from isotropic to anisotropic transport [9].

### D. Scattering Mechanisms and Relaxation Time

The effective relaxation time $\tau$ is determined by multiple scattering channels:

$$\frac{1}{\tau} = \frac{1}{\tau_{ei}} + \frac{1}{\tau_{imp}} + \frac{1}{\tau_{ph}}, \tag{9}$$

where $\tau_{ei}$, $\tau_{imp}$, and $\tau_{ph}$ correspond to electron–ion, impurity, and phonon scattering, respectively [4].


Copyright © 2025

For electron–ion scattering in a rigid lattice, the Ziman approximation [10] yields:

$$\tau_{ei}^{-1} = \frac{4\pi Z^2 e^4 \Lambda}{p_F v_F}, \tag{10}$$

with $\Lambda$ the Coulomb logarithm, and $p_F, v_F$ the Fermi momentum and velocity.

Impurity scattering is parameterized by the impurity factor $Q$:

$$\tau_{imp}^{-1} = \frac{\pi Z^2 e^4 Q}{p_F^2 v_F}, \qquad Q = \sum_j Y_j (Z_j - \langle Z \rangle)^2, \tag{11}$$

where $Y_j$ is the fractional abundance of each impurity species.

### E. Density and Magnetic Field Grid

The conductivity is evaluated across a representative range of physical conditions:

- **Density range:** $\rho = 10^9$–$4 \times 10^{11}\,\mathrm{g\,cm^{-3}}$, covering both outer and inner crust.
- **Magnetic fields:** $B = 10^{12}, 10^{13}, 10^{14}, 10^{15}\,\mathrm{G}$, representing ordinary pulsars through to strongly magnetized magnetars [11].

This grid enables a systematic study of the dependence of anisotropic conductivity on both crustal depth and magnetic field strength.

*Fiducial point for scaling plots.* For clarity in figures and scaling discussions, we highlight a fiducial point (Fe, $\rho = 10^{10}\,\mathrm{g\,cm^{-3}}$) and vary $B$ across $10^{12}$–$10^{15}$ G (SI: $10^8$–$10^{11}$ T). When captions refer to the "fiducial curve," they indicate this case.

## IV. RESULTS AND DISCUSSION

In this section, we present the results of our calculations for the electrical conductivity of neutron star crustal matter in the presence of strong magnetic fields. Employing the theoretical framework established in Section (III), we compute the three independent components of the conductivity tensor: the longitudinal conductivity ($\sigma_\parallel$), the transverse conductivity ($\sigma_\perp$), and the Hall conductivity ($\sigma_H$).

The analysis is carried out over a representative range of mass densities, $\rho = 10^9$–$4 \times 10^{11}\,\mathrm{g\,cm^{-3}}$, thereby covering the outer and inner crustal layers. The magnetic field strength is varied from $B = 10^{12}$ to $10^{15}$ G, which encompasses both the typical pulsar regime and the ultra-strong fields characteristic of magnetars.

This systematic exploration enables us to quantify the dependence of conductivity on density, magnetic field strength, and field orientation. In particular, we focus on the transition from weak to strongly magnetized regimes, the onset of significant anisotropy in electron transport, and the emergence of Hall dominance at large values of the magnetization parameter $\omega_B \tau$. The results provide direct insights into how microscopic transport properties manifest in the macroscopic thermal and magnetic evolution of neutron stars.

### A. Longitudinal Conductivity ($\sigma_\parallel$)

The longitudinal component of the electrical conductivity, aligned with the magnetic field, exhibits no appreciable dependence on field strength. As shown in Fig. 1, $\sigma_\parallel$ remains nearly constant across the entire range of densities and magnetic fields considered.

Copyright © 2025

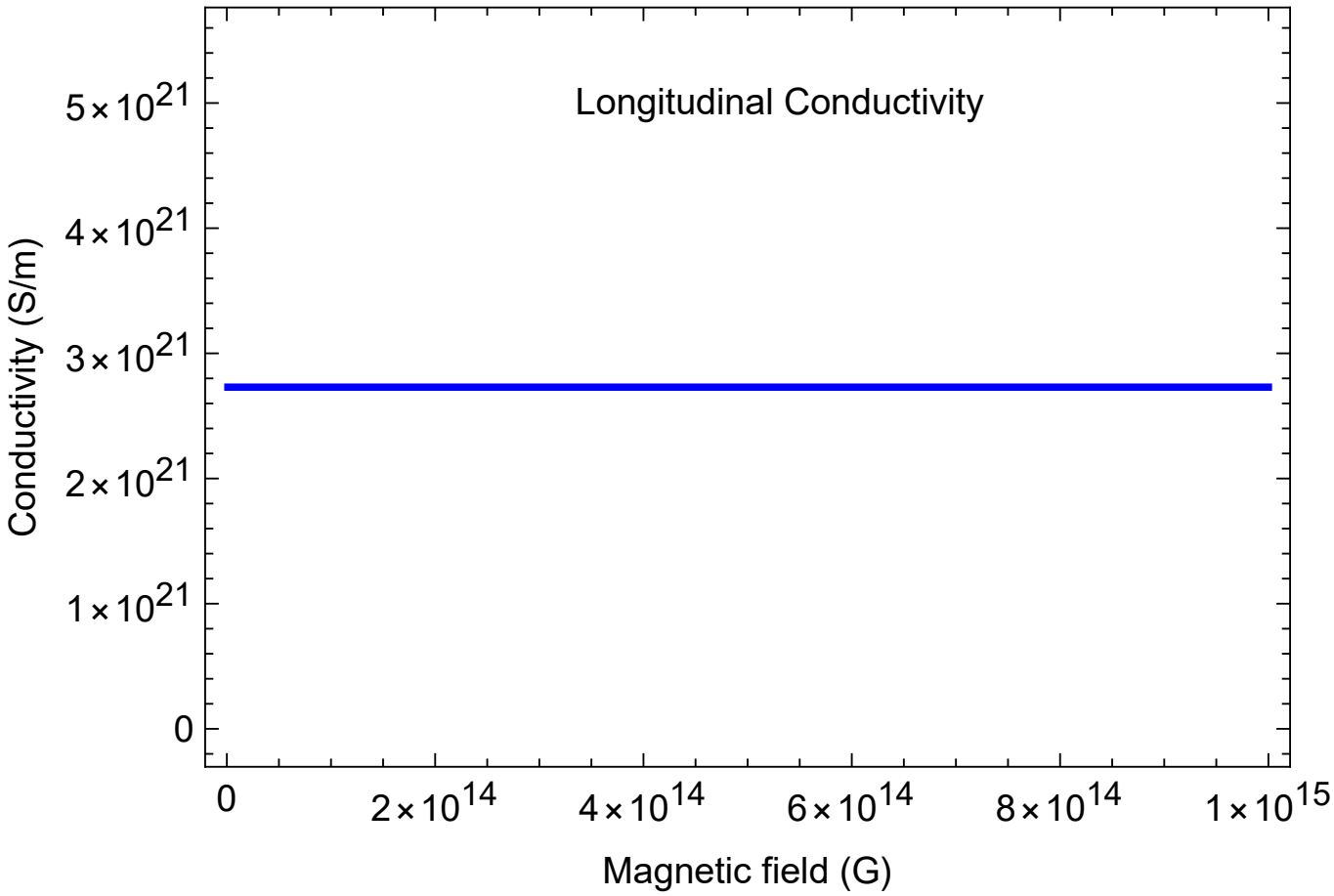



FIG. 1: **Longitudinal conductivity is insensitive to magnetic field.** The plot shows the longitudinal electrical conductivity $\sigma_{\parallel}$ of neutron–star crust matter as a function of magnetic-field strength $B$ for representative mass densities $\rho$ spanning the outer to inner crust. Across the interval $B \simeq 10^{12}$–$10^{15}$ G, the curves remain nearly flat: $\sigma_{\parallel}$ is essentially independent of $B$ because the Lorentz force does not act on motion strictly along the magnetic field. In the relaxation–time formalism, this follows from $\sigma_{\parallel} = \sigma_0 = n_e e^2 \tau / m_e^*$, which contains no $B$ dependence; the field only enters the transverse and Hall components through the magnetization parameter $\omega_B \tau = (eB/m_e^* c)\tau$. Minor variations of $\sigma_{\parallel}$ across densities reflect microphysical factors such as $n_e$ and the scattering time $\tau$ (electron–ion, impurity, or phonon scattering), rather than magnetic effects.

### B. Transverse Conductivity ($\sigma_{\perp}$)

In contrast, the transverse conductivity $\sigma_{\perp}$, which governs charge and heat transport perpendicular to the magnetic field, shows a strong dependence on field strength. As illustrated in Fig. 2, $\sigma_{\perp}$ decreases sharply once $B \gtrsim 10^{13}$ G, especially in low-density regions of the outer crust.

*Scaling with magnetic field.* From Eq. (8) and the definition of the magnetization parameter in Eq. (4), Hence, in the *strongly magnetized* limit $\omega_B \tau \gg 1$,

$$\sigma_{\perp} \simeq \frac{\sigma_0}{(\omega_B \tau)^2} \propto B^{-2} \quad \text{(for weakly } B\text{–dependent } \tau),$$

while the Hall term scales as

$$\sigma_H \simeq \frac{\sigma_0}{\omega_B \tau} \propto B^{-1}.$$

In the *weak-field* limit $\omega_B \tau \ll 1$,

$$\sigma_{\perp} \simeq \sigma_0 \left[1 - (\omega_B \tau)^2\right], \qquad \sigma_H \simeq \sigma_0 \, \omega_B \tau,$$


Copyright © 2025

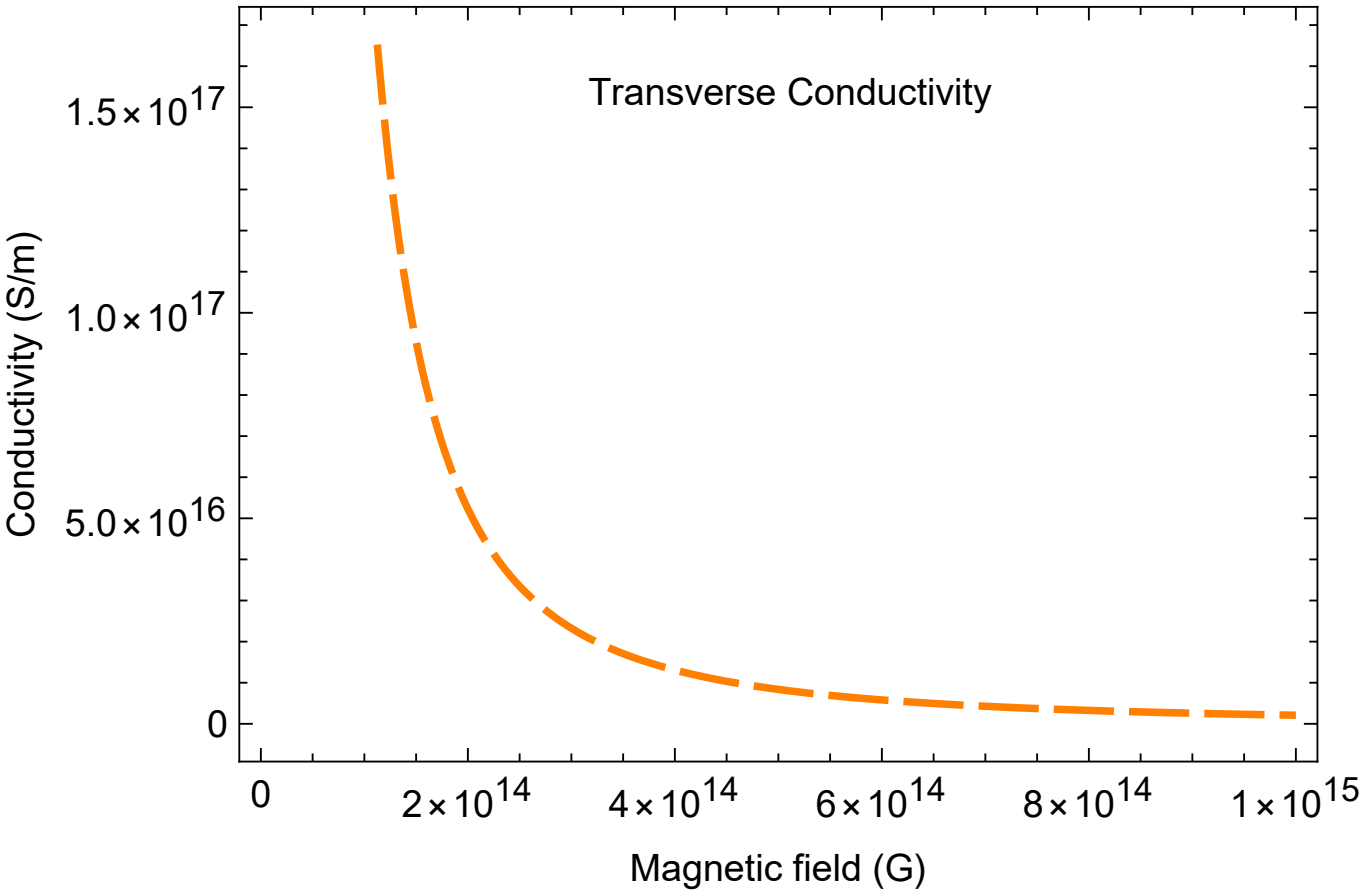



FIG. 2: **Magnetic suppression of transverse conductivity.** The transverse component of the electrical conductivity, $\sigma_\perp$, is shown as a function of magnetic-field strength $B$ for several representative mass densities of neutron-star crust matter. In contrast to the field-insensitive $\sigma_\parallel$, the quantity $\sigma_\perp$ decreases sharply once $B \gtrsim 10^{13}$ G, particularly in the low-density outer crust. This behavior, described analytically by Eq.(8), reflects the growing influence of the Lorentz force, which confines electrons to helical motion around magnetic lines and suppresses cross-field transport. Consequently, at magnetar-level fields ($B \gtrsim 10^{14}$ G), charge and heat flow become effectively channeled along the field direction.

so departures from isotropy are quadratic (for $\sigma_\perp$) and linear (for $\sigma_H$) in $B$. At the crossover $\omega_B\tau = 1$, both transverse channels are equal,

$$\sigma_\perp = \sigma_H = \frac{\sigma_0}{2},$$

marking the onset of Hall-dominated transport. For the field interval relevant here, $B : 10^{13} \to 10^{15}$ G, and for crustal conditions where $\tau$ varies only weakly with $B$ away from strong Landau-quantization features, this asymptotic scaling implies a drop in $\sigma_\perp$ by roughly $10^2 - 10^3$ and a concomitant $\sim 10 - 10^2$ decrease in $\sigma_H^{-1}$ (i.e., increase in $\sigma_H$ up to its peak and saturation thereafter). Deviations from pure power laws reflect the $B$-dependence of $\tau$ through microphysics (e.g., density of states changes in the quantizing regime).

### C. Hall Conductivity ($\sigma_H$)

The Hall component $\sigma_H$ reflects the sideways deflection of charge carriers by the Lorentz force. As shown in Fig. 3, $\sigma_H$ increases steeply with magnetic field strength at low densities, peaks when $\omega_B\tau \approx 1$, and eventually saturates for $\omega_B\tau \gg 1$.

Copyright © 2025

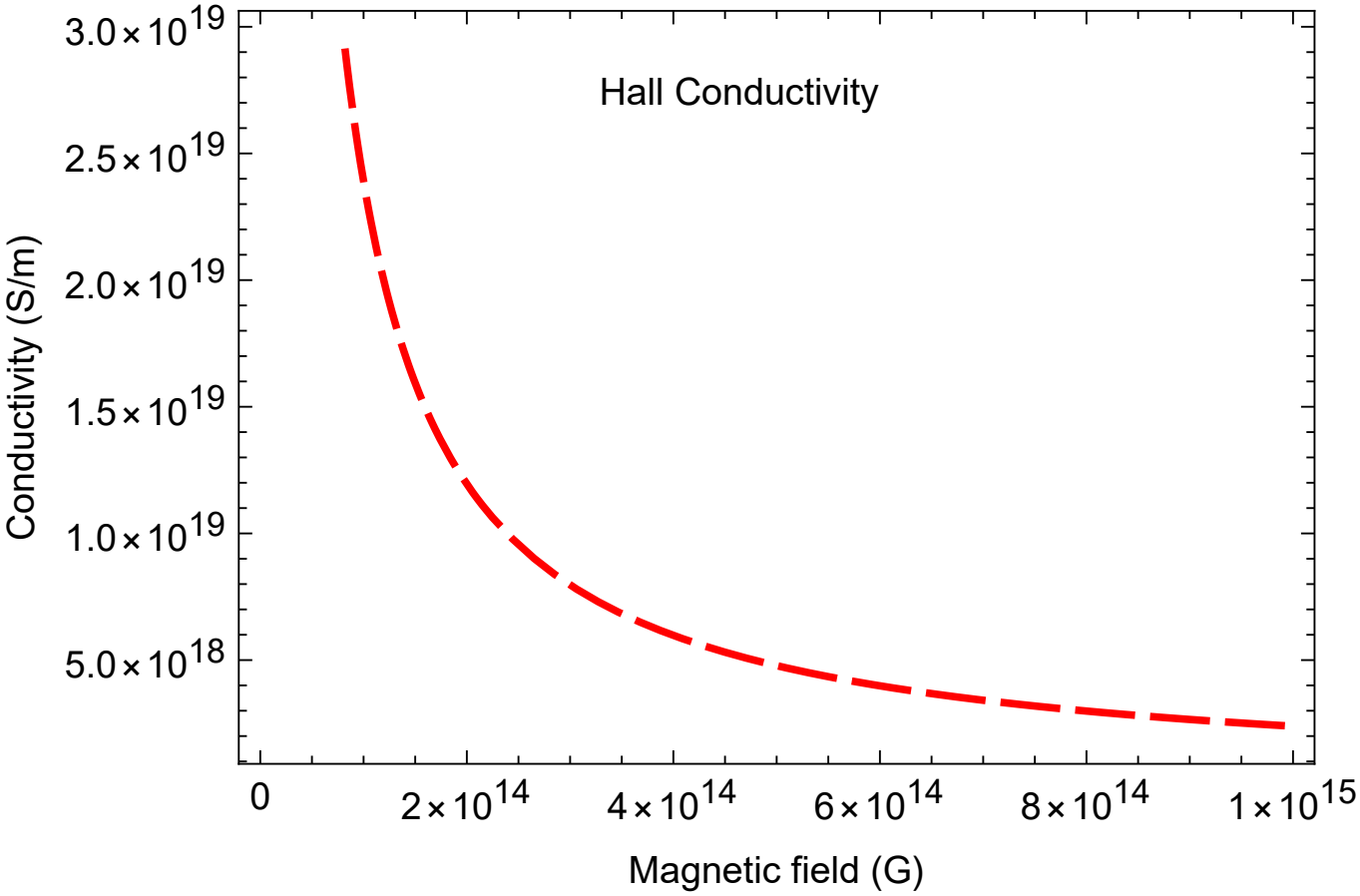



FIG. 3: **Growth and saturation of the Hall conductivity.** The Hall component of the electrical conductivity, $\sigma_{\rm H}$, is plotted versus magnetic-field strength $B$ for representative crustal densities. As indicated by Eq.(8), $\sigma_{\rm H}$ rises steeply with increasing $B$, reaching a maximum when $\omega_B\tau \approx 1$ and gradually saturating for stronger fields. This transition marks the onset of Hall-dominated transport in the outer crust. At magnetar strengths ($B \gtrsim 10^{14}$ G), $\sigma_{\rm H}$ exceeds $\sigma_\perp$ and approaches $\sigma_\parallel$, introducing nonlinear coupling into the magnetic-field evolution and enabling the formation of small-scale magnetic structures through Hall drift.

## V. INTERPRETATION AND ASTROPHYSICAL CONTEXT

The conductivity tensor obtained here implies a strongly anisotropic transport regime once the magnetization parameter exceeds unity, $\omega_B\tau \gtrsim 1$ [Eq. (4)]. From Eq. (8), the longitudinal channel remains essentially field–insensitive, $\sigma_\parallel \simeq \sigma_0$, whereas the transverse channels obey the scalings

$$\sigma_\perp \simeq \frac{\sigma_0}{1+(\omega_B\tau)^2}, \qquad \sigma_H \simeq \frac{\sigma_0\,\omega_B\tau}{1+(\omega_B\tau)^2}.$$

In the strongly magnetized limit $\omega_B\tau \gg 1$ (typical for $B \gtrsim 10^{14}$ G in the outer crust), this yields the asymptotic laws $\sigma_\perp \propto B^{-2}$ and $\sigma_H \propto B^{-1}$ (for weakly $B$-dependent $\tau$). Quantitatively, across from $10^{13}$ to $10^{15}$ G we find a suppression of cross–field conduction by $\sim 10^2 - 10^3$, while $\sigma_H$ rises, peaks near $\omega_B\tau \approx 1$, and then saturates, often exceeding $\sigma_\perp$ by an order of magnitude at $B \gtrsim 10^{14}$ G. These scalings explain why currents and heat are funneled along $\boldsymbol{B}$ and why lateral redistribution becomes Hall–dominated.

*Connection to observations.* Anisotropic transport offers a natural microscopic basis for the non-uniform surface temperature patterns inferred in several highly magnetized neutron stars. Suppressed cross-field heat flow ($\sigma_\perp \ll \sigma_\parallel$) favors warm regions magnetically connected to interior heat sources and cooler zones transverse to $\boldsymbol{B}$. In magnetars, the Hall-dominated regime ($\sigma_H \gtrsim \sigma_\perp$) also facilitates the formation and drift of small-scale magnetic structures and current sheets in the crust, which can localize heating and modulate pulse profiles.


Copyright © 2025

*Implications for magneto-thermal evolution.* Because Ohmic dissipation timescales scale with $\sigma^{-1}$, the reduction of $\sigma_\perp$ by $10^2 - 10^3$ at magnetar fields accelerates cross-field magnetic diffusion while leaving field-aligned transport efficient. The Hall term, being non-dissipative but redistributive, couples temperature and magnetic structure: it can cascade power to small scales, sharpen current layers, and seed intermittent heating. Together, these effects reshape the thermal map and the secular decay of the large-scale field, with the outer crust (low–$\rho$) typically entering the Hall-dominated regime first as $\omega_B\tau$ crosses unity.

*Direct use in simulations.* Our results can be incorporated directly into 2D/3D magneto-thermal codes by replacing the scalar conductivity with the tensor of Eq. (8). Operationally, evolve the induction equation with the generalized Ohm's law $\boldsymbol{J} = \hat{\sigma} \cdot \boldsymbol{E}'$, where $\hat{\sigma} = \begin{pmatrix} \sigma_\perp & -\sigma_H & 0 \\ \sigma_H & \sigma_\perp & 0 \\ 0 & 0 & \sigma_\parallel \end{pmatrix}$, and supply $\sigma_\parallel, \sigma_\perp, \sigma_H$ from our tables/relations as functions of $(\rho, T, B)$. In the energy equation, use $\hat{\kappa}$ consistent with $\hat{\sigma}$ (or the Wiedemann–Franz relation where applicable) to capture anisotropic heat transport. This substitution enables consistent evolution in the $\omega_B\tau \gg 1$ regime, including Hall-driven structure formation and the observed trend toward magnetically channelled surface heating.

*Scope and caveats.* The quantitative trends above hold in the cold, degenerate limit $T \ll E_F/k_B \sim 10^{12}\,\mathrm{K}$ relevant for mature crusts; at low $T$ we neglect electron–phonon scattering, so $\tau^{-1} \simeq \tau_{\mathrm{ei}}^{-1} + \tau_{\mathrm{imp}}^{-1}$. At $T \gtrsim 10^8\,\mathrm{K}$, the phonon channel should be reinstated in $\tau$, which can shift the exact crossover $\omega_B\tau \approx 1$ and slightly modify the slopes of the $\sigma_\perp(B)$ and $\sigma_H(B)$ curves. In quantizing fields ($B \gtrsim B_c$), Landau-level population alters the density of states and can imprint weak oscillatory features on the otherwise clean power-law asymptotes.

## VI. CONCLUSION

This study has examined the influence of ultra-strong magnetic fields on the electrical conductivity of neutron star crusts using a relaxation-time-based Boltzmann transport framework. By systematically evaluating the longitudinal ($\sigma_\parallel$), transverse ($\sigma_\perp$), and Hall ($\sigma_H$) components of the conductivity tensor across realistic crustal densities and magnetic field strengths ($10^{12}$–$10^{15}$ G), the analysis reveals a pronounced anisotropy that emerges once the magnetization parameter exceeds unity ($\omega_B\tau \gtrsim 1$).

The results demonstrate that longitudinal conductivity remains largely invariant with respect to magnetic field strength, whereas transverse conductivity is significantly suppressed at magnetar-level fields, particularly in the low-density outer crust. Simultaneously, the Hall conductivity increases sharply, surpassing $\sigma_\perp$ and approaching $\sigma_\parallel$ as $\omega_B\tau$ grows, signaling the transition to Hall-dominated transport. This anisotropic regime has far-reaching implications for magneto-thermal evolution, facilitating directional heat conduction, accelerating cross-field magnetic diffusion, and promoting the formation of small-scale magnetic structures through Hall drift.

These findings underscore the crucial role of magnetic-field-induced anisotropy in shaping the observable properties of neutron stars, including non-uniform surface temperature distributions, magnetic field decay, and burst activity in magnetars. Future extensions of this work should incorporate temperature-dependent scattering mechanisms, multi-component plasma compositions, and fully coupled magneto-thermal simulations to achieve a comprehensive understanding of crustal dynamics and their observational manifestations.

## REFERENCES


[1] P. Haensel, A. Y. Potekhin, and D. G. Yakovlev. *Neutron Stars 1 : Equation of State and Structure*, volume 326. 2007.

[2] Nicolas Chamel and Pawel Haensel. Physics of Neutron Star Crusts. *Living Reviews in Relativity*, 11(1):10, December 2008.

[3] A. Y. Potekhin. Electron conduction along quantizing magnetic fields in neutron star crusts. I. Theory. , 306:999, February 1996.

[4] A. Y. Potekhin, G. Chabrier, and D. G. Yakovlev. Internal temperatures and cooling of neutron stars with accreted envelopes, 1997.

[5] Arus Harutyunyan, Armen Sedrakian, Narine T. Gevorgyan, and Mekhak V. Hayrapetyan. Electrical conductivity of a warm neutron star crust in magnetic fields: Neutron-drip regime. *arXiv preprint arXiv:2309.00893*, 2023. Anisotropic conductivity tensor for inner crust; includes dynamical screening, ionic correlations, finite nuclear-size effects.

[6] Zhi-Bing Li, Xin-Jun Zhao, Wei-Feng Zhang, and Hui Wang. Magnetic Susceptibility of Relativistic Electrons in the Crust of Strongly Magnetized Neutron Stars. *Astronomische Nachrichten*, 346(7-8):e20250026, September 2025.

[7] Giorgio Almirante and Michael Urban. Superfluid fraction in the rod phase of the inner crust of neutron stars. *Phys. Rev. C*, 110(6):065802, December 2024.

[8] Dong Lai. Matter in strong magnetic fields. *Reviews of Modern Physics*, 73(3):629, July 2001.

[9] Piotr Magierski. Superfluidity in Fermi systems within the framework of Density Functional Theory. *arXiv e-prints*, page arXiv:2510.07410, October 2025.


Copyright © 2025 

[10] A. Baiko, D.˙ Effect of magnetized phonons on electrical and thermal conductivity of neutron-star crust. *Mon. Not. R. Astron. Soc.*, 458(3):2840–2856, 2016.

[11] Konstantinos N. Gourgouliatos, Davide De Grandis, and Andrei Igoshev. Magnetic Field Evolution in Neutron Star Crusts: Beyond the Hall Effect. *Symmetry*, 14(1):130, January 2022.

 Copyright © 2025